UC Irvine
UC Irvine Previously Published Works

Title

Crif1 Promotes Osteoporosis in Mice after Radiation

Permalink

Authors

Xiang, Lixin
Chen, Li
Xiang, Yang
et al.

Publication Date

DOI

Peer reviewed

1 # Crif1 Promotes Osteoporosis in Mice after Radiation

2

3 **Lixin Xiang**[1,5], **Li Chen**[1,5], **Yang Xiang**[1,2], **Fengjie Li**[1], **Xiaomei Zhang**[1], **Yanni Xiao**[1],

4 **Lingyun Zou**[3], **Jiang F. Zhong**[2], **Shengwen Calvin Li**[4], **Qian Ran**[1,2,*], **Zhongjun Li**[1,*]

5

6 1 Laboratory Medicine Center, Lab of Radiation Biology, The Second Affiliated Hospital,

7 Third Military Medical University, Chongqing 400037, China

8 2 Division of Periodontology, Diagnostic Sciences & Dental Hygiene, and Division of

9 Biomedical Sciences, Herman Ostrow School of Dentistry, University of Southern California,

10 Los Angeles, CA 90089, USA

11 3 Bioinformatics Center, College of Basic Medical Sciences, Third Military Medical

12 University, Chongqing, 400038, China

13 4 CHOC Children's Hospital Research Institute, University of California, Irvine, 1201 West

14 La Veta Ave, Orange, CA 92868, USA

15 5 These authors contributed equally to this work.

16 *Correspondense: louise-r-q@163.com (Q.R.), johnneyusc@gmail.com (Z.L.)

17
18
19
20
21
22
23
24
25
26
27
28
29
30
31
32
33
34
35
36
37
38
39

Abstract

Radiation induces rapid bone loss and enhances bone resorption and RANKL expression. RANKL provides the crucial signal to induce osteoclast differentiation and plays an important role in bone resorption. However, the mechanisms of radiation-induced osteoporosis are not fully understood. Here, we show that Crif1 expression increases in bone marrow cells after radiation. Conditional Crif1 deletion in bone marrow cells causes decreases in RANKL expression and the RANKL/OPG ratio, and relieves bone loss after radiation in mice. We further demonstrated *in vitro* that Crif1 promotes RANKL secretion via the cAMP/PKA pathway. Moreover, protein–protein docking screening identified five compounds as Crif1 inhibitors; these compounds dramatically suppressed RANKL secretion and CREB phosphorylation when cells were exposed to forskolin. This study enriches current knowledge of the pathogenesis of osteoporosis and provides insights into potential therapeutic strategies for osteoporosis treatment.

Key words   Crif1, PKA, RANKL, Osteoporosis, Radiation

Introduction

Osteoporosis is a high-incidence disease closely associated with radiotherapy, hormonal status, age and glucocorticoid treatment. It is characterized by an imbalance in skeletal turnover with reduced bone formation and enhanced bone resorption, leading to an increased risk of bone fracture(Khosla & Hofbauer, 2017; Phetfong et al., 2016). Osteoblasts are the bone-forming cells derived from bone marrow mesenchymal stem/stromal cells (BM-MSCs) and play an important role in the regulation of bone mass. Meanwhile, osteoclasts are the principal cells capable of resorbing bone and play an essential role in bone remodelling(Rachner, Khosla, & Hofbauer, 2011). Exposure to radiation, such as radiotherapy for cancer, can cause rapid mineral loss and increase the number of osteoclasts within metabolically active, cancellous bone tissue, leading to structural deficits. However, the mechanisms of radiation-induced bone loss are not fully understood. Current treatment of osteoporosis is based mainly on inhibiting bone resorption or stimulating bone generation to increase bone mass, novel treatment strategies that have a dual mechanisms should be developed.

Osteoclasts are large, multinucleated cells derived from haematopoietic progenitors of the monocyte macrophage lineage(Boyle, Simonet, & Lacey, 2003). Their differentiation is mainly regulated by macrophage colony-stimulating factor (M-CSF), RANK ligand (RANKL), and osteoprotegerin (OPG)(Teitelbaum, 2000). M-CSF is required for osteoclast survival and proliferation, but RANKL and OPG play central roles in the activation of osteoclastogenesis(Boyce & Xing, 2007). By binding to its receptor RANK (on haematopoietic progenitors), RANKL provides the crucial signal to induce osteoclast differentiation from haematopoietic progenitor cells as well as to activate mature osteoclasts. OPG is a soluble decoy receptor that can bind to RANKL and negatively regulate RANKL binding to RANK(Wada, Nakashima, Hiroshi, & Penninger, 2006). BM-MSCs, osteocytes, osteoblasts, adipocytes, and activated T and B lymphocytes are the main sources of RANKL secretion. RANKL expression is promoted by radiation, inflammation, cytokines, hormones and a number of other agents, including those that signal through cyclic adenosine monophosphate (cAMP)/protein kinase A (PKA), glycoprotein 130 (gp130) and vitamin D receptor (VDR)(Martin & Sims, 2015; Nakashima et al., 2011).

Crif1 is a multifunctional protein that can interact with many proteins to induce cell

2

87 cycle arrest, modulate oxidative stress, and regulate transcriptional activity through
88 interactions with the DNA-binding domains of transcription factors(Chen et al., 2017; Chung
89 et al., 2003; Kang, Hong, Kim, & Bae, 2010; Park et al., 2005; Ran et al., 2014). It is also the
90 constitutive protein of the large mitoribosomal subunit required for the synthesis and
91 insertion of mitochondrial-encoded OxPhos polypeptides into the mitochondrial
92 membrane(Greber et al., 2015). Crif1 deficiency in macrophages impairs mitochondrial
93 oxidative function and causes systemic insulin resistance and adipose tissue
94 inflammation(Jung et al., 2018). Our previous study showed that Crif1 promotes adipogenic
95 differentiation of BM-MSCs after radiation by modulating the cAMP/PKA signalling
96 pathway(Zhang et al., 2015).

97   In this study, we investigated the role of Crif1 in osteoporosis after radiation. To address
98 this question *in vivo*, we generated a *Crif1* bone marrow-specific conditional knockout mouse
99 model. Conditional *Crif1* deletion causes decreases in RANKL expression and the
100 RANKL/OPG ratio and reduces bone loss after radiation. In this study, we demonstrate that
101 Crif1 promotes osteoporosis by regulating RANKL expression via the cAMP/PKA pathway.
102 Through screening, we also identify five compounds that could effectively inhibit RANKL
103 expression.

104

105 **Results**

106 **Radiation induces osteoporosis in mice**

107 To confirm the extent of bone loss over the short term after irradiation, we irradiated mice
108 with a single dose of 5 Gy, and then, 7 days later, we harvested the left femurs. Micro-CT
109 analysis of the distal femurs of males and females at 12 weeks of age revealed significant
110 decreases in trabecular bone volume/total volume (BV/TV) (Figures 1A and 1B),
111 connectivity density (Conn.D) (Figure 1C), trabecular number (Tb.N*) (Figure 1D), and bone
112 mineral density (vBMD) (Figure 1E), but also showed significant increases in trabecular
113 spacing (Tb.Sp*) (Figure 1G) and structure model index (SMI) (Figure 1H). There was no
114 significant difference in trabecular thickness (Tb.Th*) (Figure 1F). Haematoxylin and eosin
115 (H&E) staining of femoral sections from irradiated mice showed significantly decreased
116 trabecular bone compared to controls (Figure 1I). Paraffin sections of femurs showed more
117 TRAP-positive cells in irradiated mice than in control mice (Figure 1J). These results
118 indicated that bone resorption was enhanced after radiation and validated the model of
119 radiation-induced osteoporosis. Moreover, RT-qPCR data revealed dramatic increases in
120 RANKL expression (Figure 1K) and the RANKL/OPG ratio in irradiated bone marrow cells
121 (Figure 1L). OPG expression was not affected by radiation treatment (Figure 1K). Notably,
122 expression of Crif1 also increased in irradiated bone marrow cells compared with control
123 cells 7 days after irradiation (Figure 1M).

124 **Conditional Crif1 deletion from bone marrow relieves bone loss after radiation**

125 To explore the possible relationship between Crif1 and RANKL, we constructed a bone
126 marrow cell-specific Crif1-deficient mouse model by crossing *Crif^{fl/fl}* mice to
127 *B6.129P2-Lyz2tm1(cre)/Nju* mice to generate *Lyz2Cre;Crif^{fl/fl}* mice (Figure 2A) and treated
128 the mice with a single dose of 5 Gy. RT-qPCR results demonstrated that *Lyz2Cre;Crif^{fl/fl}* mice
129 had lower RANKL expression (Figure 2B) and RANKL/OPG ratio in bone marrow cells
130 after radiation compared to *Crif^{fl/fl}* mice (Figure 2C). OPG expression in bone marrow cells
131 was not affected by *Crif1* deletion (Figure 2B). Therefore, we speculated that Crif1 may be
132 involved in the regulation of RANKL expression. To further assess the effects of *Crif1*
133 deletion on osteoporosis, trabecular bone parameters of femurs were evaluated by micro-CT

3

134 analysis. Conditional *Crif1* deletion from bone marrow had no effect on bone mass (Figures
135 2D-2K). Although trabecular bone volume/total volume, connectivity density and trabecular
136 number all decreased in *Crif$^{fl/fl}$* mice and *Lyz2Cre;Crif$^{fl/fl}$* mice after radiation compared to
137 nonirradiated mice, these three parameters were significantly higher in irradiated
138 *Lyz2Cre;Crif$^{fl/fl}$* mice than in irradiated *Crif$^{fl/fl}$* mice (Figures 2E ,2F and 2G). Notably,
139 trabecular spacing in *Crif$^{fl/fl}$* mice and *Lyz2Cre;Crif$^{fl/fl}$* mice both increased visibly after
140 radiation, but the increase in *Lyz2Cre;Crif$^{fl/fl}$* mice was less than that of *Crif$^{fl/fl}$* mice after
141 radiation treatment (Figure 2J). Furthermore, bone mineral density decreased (Figure 2H) and
142 structural model index increased (Figure 2K) only in irradiated *Crif$^{fl/fl}$* mice compared to
143 nonirradiated controls, while no remarkable changes in these parameters were detected
144 between nonirradiated and irradiated *Lyz2Cre;Crif$^{fl/fl}$* mice (Figure 2H and 2K). In addition,
145 trabecular thickness was not influenced by *Crif1* deletion or radiation treatment (Figure 2I).
146 H&E staining of paraffin sections of femurs confirmed the previously reported micro-CT
147 data depicting the reduced loss of trabecular tissue in *Lyz2Cre;Crif$^{fl/fl}$* mice compared to
148 *Crif$^{fl/fl}$* mice after radiation (Figure 2L). We also detected a decreased number of
149 TRAP-positive osteoclasts in irradiated *Lyz2Cre;Crif$^{fl/fl}$* mice compared to irradiated *Crif$^{fl/fl}$*
150 mice, indicating weakened bone resorption (Figure 2M). Taken together, these data suggested
151 that conditional *Crif1* deletion could alleviate bone resorption and reduce bone loss after
152 radiation.

153 **Overexpression of Crif1 in BM-MSCs increases RANKL secretion and the ratio of**
154 **RANKL to OPG**
155 To investigate the role of Crif1 in osteoporosis *in vitro*, we transfected mouse BM-MSCs
156 with a Crif1 lentiviral overexpression vector (Figure 3A). For osteoclast induction *in vitro*,
157 Crif1-overexpressing BM-MSCs and RAW264.7 cells were cocultured in a 12-well transwell
158 unit for 7 days. RT-qPCR results showed that the relative mRNA expression of RANKL and
159 RANKL/OPG ratio both increased in Crif1-overexpressing BM-MSCs compared to controls
160 after 7 days of coculture (Figure 3B and 3C). Concentrations of RANKL and OPG in
161 coculture medium were also detected by ELISA. Crif1-overexpressing BM-MSCs produced
162 high levels of RANKL compared to the control (Figure 3D), while there was no significant
163 difference in OPG concentration between the two groups (Figure 3E). The RANKL/OPG
164 ratio in Crif1-overexpressing BM-MSCs was higher than in the control (Figure 3F). We also
165 detected an increased number of tartrate-resistant alkaline phosphatase (TRAP)-positive cells
166 in RAW264.7 cells cocultured with Crif1-overexpressing BM-MSCs (Figures 3G and 3H).
167 These data suggested that Crif1 could promote RANKL expression and may be involved in
168 osteoclast differentiation.

169 **Crfi1 is involved in the regulation of RANKL expression after radiation**
170 To further confirm whether Crif1 played an important role in osteoporosis after radiation, we
171 knocked out *Crif1* in RAW264.7 cells and BM-MSCs (Figures 4A and 4D), respectively.
172 Deletion of *Crif1* from RAW264.7 cells did not affect RANK expression or osteoclast
173 differentiation (Figures 4A, 4B and 4C). We previously demonstrated that Crif1 expression
174 was upregulated after radiation(Zhang et al., 2015), and in this study, we found that RANKL
175 expression and the RANKL/OPG ratio were also elevated after radiation (Figures 4E, 4F, 4G
176 and 4I). Meanwhile, more TRAP-positive cells were found in RAW264.7 cells cocultured
177 with BM-MSCs after radiation (Figures 4J and 4K). However, knocking out *Crif1* in
178 BM-MSCs could significantly reduce RANKL expression and the RANKL/OPG ratio both
179 before and after radiation (Figures 4E, 4F, 4G and 4I). OPG expression was not affected by
180 *Crif1* deletion or radiation treatment (Figures 4E and 4H). Moreover, the number of

4

181 TRAP-positive cells also decreased in *Crif1* knockout BM-MSCs compared to the control
182 after 7 days of coculture (Figures 4J and 4K). These results further demonstrated that Crif1
183 can regulate RANKL expression, especially after radiation.

Crif1 mediates adipogenesis and RANKL secretion in adipocytes
185 To determine whether Crif1 affects RANKL expression in adipocytes, BM-MSCs were
186 grown in mouse mesenchymal stem cell adipogenic differentiation medium. Consistent with
187 our previous research(Zhang et al., 2015), more BM-MCSs became strongly predisposed to
188 adipogenesis (Figures 5A, 5B and 5C). Recently, it was reported that bone marrow
189 adipocytes can secrete RANKL(Fan et al., 2017). Here, we found an obvious increase in
190 RANKL expression and RANKL/OPG ratio in irradiated BM-MSCs after adipogenic
191 induction (Figures 5D, 5E , 5F and 5H). However, knocking out *Crif1* in BM-MSCs reduced
192 both adipogenesis and RANKL expression (Figures 5C, 5D and 5F). OPG expression was not
193 affected by *Crif1* deletion or radiation treatment (Figures 5D and 5G). These data suggested
194 that Crif1 mediates adipogenesis and RANKL secretion in adipocytes.

Crif1 promotes RANKL secretion by modulating the cAMP/PKA signalling pathway
196 To verify the mechanism underlying Crif1-mediated upregulation of RANKL expression,
197 PKA agonist (forskolin) and inhibitor (H89) were added to the coculture system. Although
198 RANKL expression and the RANKL/OPG ratio were both increased after treatment with 25
199 μM forskolin, these effects were significantly weakened in Crif1 knockout BM-MSCs
200 (Figures 6A, 6B, 6C and 6E). In addition, RANKL expression and the RANKL/OPG ratio
201 were both decreased when Crif1-overexpressing BM-MSCs and controls were treated with
202 20 μM H89 (Figures 6F, 6G , 6H and 6J). OPG expression was not affected by forskolin or
203 H89 treatment (Figures 6A, 6D, 6F and 6H). The most TRAP-positive cells were found in the
204 coculture with forskolin-treated BM-MSCs (Figures 6K and 6L), the fewest TRAP-positive
205 cells were found in the coculture with H89-treated cells (Figures 6M and 6N). After the
206 addition of forskolin, CREB phosphorylation was significantly increased in the control
207 BM-MSCs, but was dramatically inhibited in *Crif1* knockout BM-MCSs (Figure 6O). We
208 also observed that CREB phosphorylation was suppressed in both Crif1-overexpressing
209 BM-MSCs and controls following exposure to H89 (Figure 6P). These results demonstrated
210 that Crif1 promotes RANKL expression through cAMP/PKA signalling pathway.

Crif1 inhibitors effectively suppress RANKL secretion and CREB phosphorylation
212 We used ClusPro and InterProSurf to investigate the interface in Crif1-PKAα complex, and
213 results showed that Thr[197], Gly[200], Thr[201], Glu[203], and Phe[129] of PKAα interact with Ile[132],
214 Met[128], Ile[121], His[120], and Arg[117] in the long alpha helical region of Crif1, forming the binding
215 interface (Figure 7A). A virtual screening using 462,608 compounds from the Life Chemicals
216 database around His[120] of Crif1 was carried out using the program Autodock_vina. A set of
217 13 compounds was selected for experimental screening based on binding energy <-12.0
218 kcal/mol (Table S1). Initially a tetrazolium salt (WST-8) assay was carried out to study
219 potential toxic effects of these compounds on hBM-MSCs, vero cells and mouse BM-MSCs
220 (Figures S1-S3). The compounds F0382-0033, F3408-0076, F1430-0134, F3408-0031 and
221 F1430-0130 showed low toxicity to hBM-MSCs at concentrations of 25 μM (Figure 7G-7K).
222 The binding pattern in these ligand−protein complexes potentially contained multiple
223 interactions dominated by hydrophobic amino acids (Figure 7B-7F). To determine whether
224 these 5 Crif1 inhibitors affected RANKL expression, hBM-MSCs were pretreated with these
225 compounds followed by treatment with forskolin. ELISA analysis of supernatant medium
226 revealed that RANKL expression was dramatically decreased by treatment with Crif1
227 inhibitors (Figure 7L). OPG expression could be significantly increased by F1430-0134

5

228   (Figure 7M). Moreover, RANKL/OPG ratios were also decreased by these 5 inhibitors
229   (Figure 7N). To further understand the mechanism, CREB phosphorylation was detected.
230   Western blotting analysis showed that CREB phosphorylation was inhibited by treatment
231   with the 5 inhibitors that showed suppressive effects on RANKL expression (Figure 7O).

232   **Discussion**

233   Radiation exposure (due to radiotherapy, accidental causes or terrorism) causes
234   irreparable damage to tissues and organs such as bone marrow. It suppresses bone formation
235   and elevates resorption, disturbing the balance between them and leading to a dramatic
236   decline in trabecular bone(D'Oronzo, Stucci, Tucci, & Silvestris, 2015; Jia, Gaddy, Suva, &
237   Corry, 2011). In this study, we treated mice with a single dose of 5 Gy to generate a model of
238   radiation-induced osteoporosis. RANKL expression and RANKL/OPG ratios actually
239   increased in the surviving bone marrow cells after radiation, which was consistent with a
240   previous study(Alwood et al., 2015). Meanwhile, expression of Crif1 and bone resorption
241   also increased, indicating a relationship between RANKL and Crif1 in osteoporosis.
242   BM-MSCs, osteoblasts, adipocytes and activated T lymphocytes in bone marrow are the
243   main source of RANKL secretion(Boyce & Xing, 2008; Honma et al., 2013); thus, to
244   elucidate the possible role of Crif1 in RANKL expression, we generated bone marrow
245   cell-specific Crif1-deficient mice. Conditional *Crif1* deletion from bone marrow could reduce
246   RANKL expression and relieve bone loss after radiation, suggesting that Crif1 is involved in
247   RANKL expression and osteoporosis.

248   BM-MSCs, which are a major and important component of the haematopoietic
249   microenvironment, secrete soluble RANKL and OPG(Horowitz, Xi, Wilson, & Kacena, 2001;
250   Morrison & Scadden, 2014). In our study, overexpression of Crif1 in BM-MSCs resulted in
251   an increase in RANKL secretion, while deletion of Crif1 from BM-MSCs significantly
252   reduced RANKL expression. BM-MSCs are pluripotent and are the progenitors of both bone
253   marrow osteocytes and adipocytes. The balance between osteogenic and adipogenic
254   differentiation of BM-MSCs also plays a pivotal role in maintaining bone homeostasis(Mori
255   et al., 2014; Yue, Zhou, Shimada, Zhao, & Morrison, 2016). Excessive numbers of
256   adipocytes are often found in the bone marrow of patients with osteoporosis. A recent study
257   revealed that bone marrow adipocytes can also secrete RANKL and accelerate
258   osteoclastogenesis(Fan et al., 2017). Moreover, after radiation exposure, the haematopoietic
259   red marrow gradually turns to yellow, a phenomenon known as bone marrow fatting.
260   Compared to other cells in bone marrow, BM-MSCs are more resistant to radiation; however,
261   radiation impairs the balance between osteogenic and adipogenic differentiation of
262   BM-MSCs, decreasing osteogenesis while increasing RANKL expression and
263   adipogenesis(Cao et al., 2011). We previously reported that Crif1 can promote the
264   adipogenesis of BM-MSCs. Here, we found that deletion of Crif1 from BM-MSCs can
265   reduce both adipogenesis and RANKL expression. Osteogenesis and adipogenesis in the
266   bone marrow are inversely correlated, so reduced adipogenesis results in an increase in the
267   osteoblast pool(Muruganandan, Roman, & Sinal, 2009; Nuttall & Gimble, 2000).

268   RANKL functions as an osteoclast-activating factor, and its binding to RANK induces
269   the activation of transcription factors such as c-fos, NFAT, and nuclear factor kappa B
270   (NF-κB) in preosteoclasts and initiates several downstream signalling pathways, especially
271   the NF-κB pathway(Nakashima, Hayashi, & Takayanagi, 2012). RANKL expression can be
272   upregulated by many agents, such as PTH and forskolin. Forskolin can stimulate RANKL
273   expression through the cAMP/PKA signalling pathway(Kondo, Guo, & Bringhurst, 2002;
274   Tseng et al., 2010). However, deletion of Crif1 from BM-MSCs impairs the promotion of

275 RANKL expression by forskolin. Moreover, overexpression of Crif1 in BM-MSCs does not
276 increase RANKL expression upon exposure to a PKA inhibitor. Our previous study revealed
277 that Crif1 can interact with PKA and promote adipogenesis. Here, we further demonstrated
278 that Crif1 can also promote RANKL expression through the cAMP/PKA signalling pathway.

279   Drugs for the treatment of osteoporosis could be divided into anabolic and antiresorptive
280 categories. Bisphosphonates (including alendronate and ibandronate), oestrogen, selective
281 oestrogen receptor modulators (SERMs), and denosumab are antiresorptive drugs, whereas
282 parathyroid hormone (PTH) and its analogues are anabolic agents(Andreopoulou & Bockman,
283 2015; Favus, 2010; Torstrick & Guldberg, 2014). However, the long-term adverse effects of
284 these anti-osteoporotic drugs should be considered, such as hypocalcaemia, arthralgia, nausea,
285 and especially the development of breast cancer and risks of cardiovascular events and
286 thromboembolism associated with treatment with oestrogen and SERMs(Black & Rosen,
287 2016; Khan, Cheung, & Khan, 2017). Therefore, it is necessary to look for new drugs with
288 high efficiency but few side effects. Because of the importance of RANKL in osteoclast
289 differentiation, RANKL-secreting cells, which play a central role in osteoclastogenesis, are
290 the targets of most antiresorptive agents(Dempster, Lambing, Kostenuik, & Grauer, 2012;
291 Tella & Gallagher, 2014). Future drug screening should target not only the regulation of the
292 balance between bone formation and bone resorption but also the balance between osteogenic
293 and adipogenic differentiation. Here, through screening, we identified five compounds that
294 effectively inhibit Crif1 activity in the cAMP/PKA signalling pathway. These five
295 compounds may have dual actions on bone metabolism, both increasing bone formation and
296 decreasing bone resorption and adipogenesis.

297   In summary, we demonstrated that Crif1 plays a crucial role in osteoporosis and that
298 conditional *Crif1* deletion reduces bone loss after radiation. Moreover, through screening, we
299 identified five Crif1 inhibitors that could dramatically reduce RANKL secretion and CREB
300 phosphorylation. This study enriches current knowledge of the pathogenesis of
301 radiation-induced osteoporosis and provides insights into potential therapeutic strategies for
302 osteoporosis treatment.

303 **Materials and Methods**
304 **Mouse Strains**
305 Male and female C57BL/6 mice (aged 12-14 weeks) were purchased from Beijing HFK
306 Bio-Technology Co. Ltd. *B6.129P2-Lyz2tm1(cre)/Nju* mice were received as a gift from
307 Assistant Professor Tao Wang (Third Military Medical University). *Crif$^{fl/fl}$* mice were
308 constructed by Nanjing BioMedical Research Institute of Nanjing University (NBRI).
309 *Lyz2Cre;Crif1$^{fl/fl}$* mice were generated by crossing *Crif$^{fl/fl}$* mice to
310 *B6.129P2-Lyz2tm1(cre)/Nju* transgenic mice. For radiation treatment, mice were irradiated
311 with 5 Gy Co-60 at a rate of 0.69 Gy/minute. Blood was collected at 7 days after irradiation,
312 and serum from each mouse was analysed individually in triplicate.

313 **Cell culture and treatment**
314 For *in vitro* study, mouse bone marrow mesenchymal stem/stromal cells (BM-MSCs)
315 purchased from Cyagen Biosciences were cultured in mouse mesenchymal stem cell medium
316 (MUCMX-90011, Cyagen Biosciences) at 37℃ and 5% CO_2. For radiation treatment, mouse
317 BM-MSCs were irradiated with 9 Gy Co-60 at a rate of 0.69 Gy/minute.
318 RAW264.7 cells were cultured in Dulbecco's modified Eagle medium (DMEM, HyClone)
319 supplemented with 10% FBS.
320 For osteoclast induction, RAW264.7 cells and mouse BM-MSCs were cocultured in a
321 12-well transwell unit (0.4 μm) for 7 days with or without forskolin (25 μM) or H89 (20 μM)

7

322 treatment. After 7 days of coculture, cells were collected for RT-qPCR and Western blotting;
323 meanwhile, supernatant medium was collected for ELISA.
324 Human bone marrow mesenchymal stem/stromal cells (hBM-MSCs) (catalogue No. 7500,
325 ScienCell) were cultured in mesenchymal stem cell medium (catalogue No. 7501, ScienCell)
326 at 37 ℃ and 5% CO_2.

Crif1 knockout and overexpression in vitro

328 For Crif1 overexpression, mouse BM-MSCs were transfected with a Crif1 lentiviral
329 overexpression vector (pLV[Exp]-EGFP:T2A:Puro-EF1A>mGadd45gip1
330 [NM_183358.4]) constructed by Cyagen Biosciences (vector ID: VB180112-1182ypt) and
331 selected with 5 μg/ml puromycin dihydrochloride (A1113803, Invitrogen). An empty vector
332 (pLV[Exp]-EGFP:T2A:Puro-Null, vector ID: VB160420-1011mqh, Cyagen Biosciences) was
333 included as a control.
334 For *Crif1* knockout, mouse BM-MSCs were first transfected with lentiCas9-Blast vector
335 (Genomeditech) and selected with 5 μg/ml blasticidin S HCl (A1113903, Invitrogen). Then,
336 cells were transfected with CRISPR/Cas9 M_Gadd45gip1 gRNA vector (target sequence:
337 GCGGGGGCGCACGGTAGCTG, Genomeditech) and selected with 5 μg/ml puromycin
338 dihydrochloride. An empty vector (LentiGuide-Puro-Scramble-gRNA, Genomeditech) was
339 included as a control.

In vitro adipogenic differentiation

341 To induce adipogenesis, mouse BM-MSCs were treated in mouse mesenchymal stem cell
342 adipogenic differentiation medium (MUCMX-90031, Cyagen Biosciences). After
343 differentiation, we preserved the supernatant medium for ELISA and fixed the cells
344 with 2 ml of 4% formaldehyde solution for 30 minutes. Then, the cells were stained with 1
345 ml oil red O working solution (catalogue No. S0131, Cyagen Biosciences) for 30 minutes and
346 visualized with a light microscope (Leica DMIRB, Heidelberg, Germany). The dye from oil
347 red O staining was extracted using isopropanol, and the optical density at 510 nm was
348 measured using a Varioskan FLASH microplate reader.

Micro-CT analysis

350 Femurs were dissected, fixed overnight in 4% paraformaldehyde, and stored in 1%
351 paraformaldehyde at 4℃. Trabecular bone parameters were measured in the distal metaphysis
352 of the femur. We started analysing slices at the bottom of the distal growth plate, where the
353 epiphyseal cap structure completely disappeared and continued for 95 slices (10.5 μm/slice,
354 using SCANCO VivaCT40) towards the proximal end of the femur.

Isolation of bone marrow cells

356 Femurs were collected and cleaned in sterile PBS, and both ends of each femur were trimmed
357 off. Bones were placed in a 0.6-mL microcentrifuge tube that was cut open at the bottom and
358 nested inside a 1.5-mL microcentrifuge tube. Fresh bone marrow was spun out by brief
359 centrifugation (from 0 to 10,000 rpm, 9 s). Red blood cells were lysed using RBC lysis buffer
360 (catalogue NO. RT122-02, TIANGEN). After centrifugation (3,000 rpm, 5 minutes), cells at
361 the bottom layer were collected for Western blotting and RT-qPCR assays(Fan et al., 2017).

Western blotting and antibodies

363 Protein expression in the samples was analysed by Western blotting. Total protein lysates
364 were extracted with cell lysis buffer for Western blotting and immunoprecipitation (catalogue
365 No. P0013, Beyotime) and denatured by boiling. Protein samples were resolved on 12%
366 SDS-polyacrylamide gels and transferred to polyvinylidene fluoride membranes (PVDF
367 Western Blotting Membranes; Roche). Membranes were blocked in PBS containing 5% (w/v)
368 nonfat dry milk and 0.1% TWEEN 20 and then incubated with the appropriate primary

369 antibodies overnight at 4 ℃. Membranes were washed with TBST three times, and then
370 incubated with the appropriate horseradish peroxidase-conjugated secondary antibodies for 1
371 h at 24 ℃. Immunoreactive bands were detected by the BeyoECL Plus reagent (P0018,
372 Beyotime) using a Photo-Image System (Molecular Dynamics, Sunnyvale, CA, USA). The
373 primary antibodies used for blotting were as follows: Crif1 (M-222) (sc-134882; Santa Cruz),
374 RANK (H-7) (sc-374360; Santa Cruz), A-FABP (AP2, sc-18661; Santa Cruz), PPARγ
375 (sc-7273; Santa Cruz), β-actin (sc-47778; Santa Cruz), phospho-CREB rabbit mAb (#9198;
376 Cell Signaling Technology), and CREB rabbit mAb (#9197; Cell Signaling Technology).

377 **RT-qPCR**
378 Real-time quantitative polymerase chain reaction (RT-qPCR) was used to analyse the mRNA
379 levels of selected genes in collected samples. Total RNA was extracted using TRIzol Reagent
380 (catalogue No. 10296010, Invitrogen) according to the manufacturer's instructions.
381 First-strand cDNA was synthesized from l μg of RNA using the PrimeScript RT Reagent Kit
382 with gDNA Eraser (catalogue No. RR047A, TaKaRa). qPCR was performed in triplicate in
383 20- μl reactions containing SYBR Premix Ex Taq II (catalogue No. RR820A, TaKaRa). The
384 reaction protocol was as follows: heating for 30 s at 95℃, followed by 40 cycles of
385 amplification (5 s at 95℃, 30 s at 60℃).
386 The sequences of the RT-PCR primers were as follows:
387 M-actin-F: AGCCATGTACGTAGCCATCC,
388 M-actin-R: CTCAGCTGTGGTGGTGAA,
389 M-Rankl-F: GCTCCGAGCTGGTGAAGAAA,
390 M-Rankl-R:CCCCAAAGTACGTCGCATCT,
391 M-OPG-F: GTTCCTGCACAGCTTCACAA,
392 M-OPG-R: AAACAGCCCAGTGACCATTC.

393 **ELISA**
394 The concentrations of RANKL and OPG were measured using the Mouse RANκL (Receptor
395 Activator of Nuclear Factor Kappa B Ligand) ELISA Kit (E-EL-M0644c, elabscience),
396 Human sRANKL (Soluble Receptor Activator of Nuclear factor-kB Ligand) ELISA Kit
397 (E-EL-H5558c, elabscience), Mouse OPG (Osteoprotegerin) ELISA Kit (E-EL-M0081c,
398 elabscience) and Human OPG (Osteoprotegerin) ELISA Kit (E-EL-H1341c, elabscience)
399 according to the manufacturer's instructions. Assays were performed in triplicate.

400 **Tartrate-resistant acid phosphatase (TRAP) staining**
401 After the 7-day coculture period, cells were washed once with PBS, fixed in 10% formalin
402 for 10 minutes, and incubated with a substrate solution, naphthol AS-BI phosphate (catalogue
403 No. 387, Sigma), in the presence of 50 mM sodium tartrate at 37 ℃ for 1 h. The resulting
404 mononuclear and multinuclear TRAP-positive cells were visualized by light microscopy and
405 quantified.

406 **Histochemistry and histomorphometric analysis**
407 Femurs were dissected, fixed overnight in 4% paraformaldehyde, decalcified in 10% EDTA
408 (pH 7.0) for 20 days and embedded in paraffin. Longitudinally oriented sections of bone 4
409 μm thick, including the metaphysis and diaphysis, were processed for histochemistry and
410 haematoxylin and eosin (H&E) staining. Dewaxed sections were also stained for
411 tartrate-resistant acid phosphatase (TRAP) activity to identify osteoclasts. Sections were
412 incubated in TRAP stain for 45 minutes at 37℃.

413 **Crif1 inhibitor screening**
414 ClusPro and InterProSurf were used to investigate the interface in Crif1-PKAα complex. A
415 virtual screening using 462,608 compounds from the Life Chemicals database around His[120]

9

416   of Crif1 was carried out using the program Autodock_vina. For inhibitor screening,

417   hBM-MSCs were cultured in 6-well plates and pretreated with 5 different compounds (25

418   μM). After 3 hours of pretreatment, forskolin (25 μM) was added to the medium. After 1

419   hour of forskolin treatment, total protein lysates were extracted for CREB phosphorylation

420   detection, and 3 days later, supernatant medium was collected for ELISA.

421   **Tetrazolium salt (WST-8) assay**

422   A tetrazolium salt (WST-8) assay was carried out to study the toxicity of compounds to

423   hBM-MSCs. hBM-MSCs seeded at a density of 3000 cells per well in 96-well plate were

424   treated with 5 different compounds at 8 final concentrations (3.125 μM, 6.25 μM, 12.5 μM,

425   25 μM, 50 μM, 100 μM, 200 μM, 400 μM). Three days later, 10 μl cell counting kit-8 solution

426   was added to each well. After 4 hours of incubation, the absorbance at 450 nm was measured

427   using a Varioskan FLASH microplate reader (Thermo).

428   **Statistical analysis**

429   The mRNA expression levels of RANKL and OPG in the tested samples were determined as

430   the cycle threshold (CT) level, and normalized copy numbers (relative quantification) were

431   calculated using the $\Delta\Delta$CT equation as follows: $\Delta\Delta$CT=ΔCT of the bone marrow sample

432   -ΔCT of β-actin, and then the normalized copy number (relative quantification)=$2^{-\Delta\Delta CT}$. Data

433   are presented as the mean±SD. Statistical significance was assessed using a two-tailed paired

434   Student's t-test. The results were considered significant when * $p<0.05$ or ** $p<0.01$.

435   **Study approval**

436   All animal studies performed were approved by the Institutional Animal Care and Use

437   Committee at the Third Military Medical University.

442   **Author Contributions**: Z.L., L.X., Q.R. and L.C.: conceived the project; L.X. and Q.R.:

443   designed and performed most experiments and data analysis with input; Y.X., F.L., M.Z.,

444   L.C., Y.X., L.Z., J.F.Z. and S.C.L.: assisted with experiments; L.X.: wrote and edited the

445   manuscript.

446   **Declaration of Interests:** The authors have declared that no conflict of interest exists.

447   **References**

448   Alwood, J. S., Shahnazari, M., Chicana, B., Schreurs, A. S., Kumar, A., Bartolini, A., . . .

449   Globus, R. K. (2015). Ionizing Radiation Stimulates Expression of

450   Pro-Osteoclastogenic Genes in Marrow and Skeletal Tissue. *J Interferon Cytokine*

451   *Res, 35*(6), 480-487. doi:10.1089/jir.2014.0152

452   Andreopoulou, P., & Bockman, R. S. (2015). Management of postmenopausal osteoporosis.

453   *Annu Rev Med, 66*, 329-342. doi:10.1146/annurev-med-070313-022841

454   Black, D. M., & Rosen, C. J. (2016). Postmenopausal Osteoporosis. *N Engl J Med, 374*(21),

455   2096-2097. doi:10.1056/NEJMc1602599

456   Boyce, B. F., & Xing, L. (2007). Biology of RANK, RANKL, and osteoprotegerin. *Arthritis Res*

457   *Ther, 9 Suppl 1*, S1. doi:10.1186/ar2165

458   Boyce, B. F., & Xing, L. (2008). Functions of RANKL/RANK/OPG in bone modeling and

459   remodeling. *Arch Biochem Biophys, 473*(2), 139-146.

460   doi:10.1016/j.abb.2008.03.018

461 Boyle, W. J., Simonet, W. S., & Lacey, D. L. (2003). Osteoclast differentiation and activation.
462   *Nature, 423*(6937), 337-342. doi:10.1038/nature01658

463 Cao, X., Wu, X., Frassica, D., Yu, B., Pang, L., Xian, L., . . . Frassica, F. J. (2011). Irradiation
464   induces bone injury by damaging bone marrow microenvironment for stem cells.
465   *Proc Natl Acad Sci U S A, 108*(4), 1609-1614. doi:10.1073/pnas.1015350108

466 Chen, L., Ran, Q., Xiang, Y., Xiang, L., Li, F., Wu, J., . . . Li, Z. (2017). Co-Activation of PKC-δ
467   by CRIF1 Modulates Oxidative Stress in Bone Marrow Multipotent Mesenchymal
468   Stromal Cells after Irradiation by Phosphorylating NRF2 Ser40. *Theranostics, 7*(10),
469   2634-2648. doi:10.7150/thno.17853

470 Chung, H. K., Yi, Y. W., Jung, N. C., Kim, D., Suh, J. M., Kim, H., . . . Shong, M. (2003).
471   CR6-interacting factor 1 interacts with Gadd45 family proteins and modulates the
472   cell cycle. *J Biol Chem, 278*(30), 28079-28088. doi:M212835200 [pii]
473 10.1074/jbc.M212835200

474 D'Oronzo, S., Stucci, S., Tucci, M., & Silvestris, F. (2015). Cancer treatment-induced bone
475   loss (CTIBL): pathogenesis and clinical implications. C*ancer Treat Rev, 41(*9),
476   798-808. doi:10.1016/j.ctrv.2015.09.003

477 Dempster, D. W., Lambing, C. L., Kostenuik, P. J., & Grauer, A. (2012). Role of RANK ligand
478   and denosumab, a targeted RANK ligand inhibitor, in bone health and osteoporosis:
479   a review of preclinical and clinical data. C*lin Ther, 34(*3), 521-536.
480   doi:10.1016/j.clinthera.2012.02.002

481 Fan, Y., Hanai, J. I., Le, P. T., Bi, R., Maridas, D., DeMambro, V., . . . Lanske, B. (2017).
482   Parathyroid Hormone Directs Bone Marrow Mesenchymal Cell Fate. C*ell Metab,
483   25(3*), 661-672. doi:10.1016/j.cmet.2017.01.001

484 Favus, M. J. (2010). Bisphosphonates for osteoporosis. N *Engl J Med, 363(*21), 2027-2035.
485   doi:10.1056/NEJMct1004903

486 Greber, B. J., Bieri, P., Leibundgut, M., Leitner, A., Aebersold, R., Boehringer, D., & Ban, N.
487   (2015). Ribosome. The complete structure of the 55S mammalian mitochondrial
488   ribosome. S*cience, 348(*6232), 303-308. doi:10.1126/science.aaa3872

489 Honma, M., Ikebuchi, Y., Kariya, Y., Hayashi, M., Hayashi, N., Aoki, S., & Suzuki, H. (2013).
490   RANKL subcellular trafficking and regulatory mechanisms in osteocytes. J *Bone
491   Miner Res, 28(*9), 1936-1949. doi:10.1002/jbmr.1941

492 Horowitz, M. C., Xi, Y., Wilson, K., & Kacena, M. A. (2001). Control of osteoclastogenesis
493   and bone resorption by members of the TNF family of receptors and ligands.
494   C*ytokine Growth Factor Rev, 12(*1), 9-18.

495 Jia, D., Gaddy, D., Suva, L. J., & Corry, P. M. (2011). Rapid loss of bone mass and strength
496   in mice after abdominal irradiation. R*adiat Res, 176(*5), 624-635.

497 Jung, S. B., Choi, M. J., Ryu, D., Yi, H. S., Lee, S. E., Chang, J. Y., . . . Shong, M. (2018).
498   Reduced oxidative capacity in macrophages results in systemic insulin resistance.
499   N*at Commun, 9(*1), 1551. doi:10.1038/s41467-018-03998-z

500 Kang, H. J., Hong, Y. B., Kim, H. J., & Bae, I. (2010). CR6-interacting factor 1 (CRIF1)
501   regulates NF-E2-related factor 2 (NRF2) protein stability by proteasome-mediated
502   degradation. J *Biol Chem, 285(*28), 21258-21268. doi:M109.084590 [pii]
503 10.1074/jbc.M109.084590

504 Khan, M., Cheung, A. M., & Khan, A. A. (2017). Drug-Related Adverse Events of
505   Osteoporosis Therapy. En*docrinol Metab Clin North Am, 46(1*), 181-192.
506   doi:10.1016/j.ecl.2016.09.009

507   Khosla, S., & Hofbauer, L. C. (2017). Osteoporosis treatment: recent developments and
508   ongoing challenges. La*ncet Diabetes Endocrinol, 5(1*1), 898-907.
509   doi:10.1016/S2213-8587(17)30188-2

510   Kondo, H., Guo, J., & Bringhurst, F. R. (2002). Cyclic adenosine monophosphate/protein
511   kinase A mediates parathyroid hormone/parathyroid hormone-related protein
512   receptor regulation of osteoclastogenesis and expression of RANKL and
513   osteoprotegerin mRNAs by marrow stromal cells. J *Bone Miner Res, 17(9*),
514   1667-1679. doi:10.1359/jbmr.2002.17.9.1667

515   Martin, T. J., & Sims, N. A. (2015). RANKL/OPG; Critical role in bone physiology. Re*v Endocr*
516   *Metab Disord, 16(2*), 131-139. doi:10.1007/s11154-014-9308-6

517   Mori, K., Suzuki, K., Hozumi, A., Goto, H., Tomita, M., Koseki, H., . . . Osaki, M. (2014).
518   Potentiation of osteoclastogenesis by adipogenic conversion of bone
519   marrow-derived mesenchymal stem cells. Bi*omed Res, 35(2*), 153-159.

520   Morrison, S. J., & Scadden, D. T. (2014). The bone marrow niche for haematopoietic stem
521   cells. Na*ture, 505(7*483), 327-334. doi:10.1038/nature12984

522   Muruganandan, S., Roman, A. A., & Sinal, C. J. (2009). Adipocyte differentiation of bone
523   marrow-derived mesenchymal stem cells: cross talk with the osteoblastogenic
524   program. Ce*ll Mol Life Sci, 66(2*), 236-253. doi:10.1007/s00018-008-8429-z

525   Nakashima, T., Hayashi, M., Fukunaga, T., Kurata, K., Oh-Hora, M., Feng, J. Q., . . .
526   Takayanagi, H. (2011). Evidence for osteocyte regulation of bone homeostasis
527   through RANKL expression. Na*t Med, 17(1*0), 1231-1234. doi:10.1038/nm.2452

528   Nakashima, T., Hayashi, M., & Takayanagi, H. (2012). New insights into osteoclastogenic
529   signaling mechanisms. Tr*ends Endocrinol Metab, 23(1*1), 582-590.
530   doi:10.1016/j.tem.2012.05.005

531   Nuttall, M. E., & Gimble, J. M. (2000). Is there a therapeutic opportunity to either prevent
532   or treat osteopenic disorders by inhibiting marrow adipogenesis? Bo*ne, 27(2*),
533   177-184.

534   Park, K. C., Song, K. H., Chung, H. K., Kim, H., Kim, D. W., Song, J. H., . . . Shong, M. (2005).
535   CR6-interacting factor 1 interacts with orphan nuclear receptor Nur77 and inhibits
536   its transactivation. Mo*l Endocrinol, 19(1*), 12-24. doi:10.1210/me.2004-0107

537   Phetfong, J., Sanvoranart, T., Nartprayut, K., Nimsanor, N., Seenprachawong, K.,
538   Prachayasittikul, V., & Supokawej, A. (2016). Osteoporosis: the current status of
539   mesenchymal stem cell-based therapy. Ce*ll Mol Biol Lett, 21,* 12.
540   doi:10.1186/s11658-016-0013-1

541   Rachner, T. D., Khosla, S., & Hofbauer, L. C. (2011). Osteoporosis: now and the future.
542   La*ncet, 377(9*773), 1276-1287. doi:10.1016/S0140-6736(10)62349-5

543   Ran, Q., Hao, P., Xiao, Y., Xiang, L., Ye, X., Deng, X., . . . Li, Z. (2014). CRIF1 interacting with
544   CDK2 regulates bone marrow microenvironment-induced G0/G1 arrest of leukemia
545   cells. PL*oS One, 9(2*), e85328. doi:10.1371/journal.pone.0085328

546   Teitelbaum, S. L. (2000). Bone resorption by osteoclasts. Sc*ience, 289(5*484), 1504-1508.

547   Tella, S. H., & Gallagher, J. C. (2014). Prevention and treatment of postmenopausal
548   osteoporosis. J *Steroid Biochem Mol Biol, 142,* 155-170.
549   doi:10.1016/j.jsbmb.2013.09.008

550   Torstrick, F. B., & Guldberg, R. E. (2014). Local strategies to prevent and treat osteoporosis.
551   Cu*rr Osteoporos Rep, 12(1*), 33-40. doi:10.1007/s11914-014-0191-6

552   Tseng, W., Graham, L. S., Geng, Y., Reddy, A., Lu, J., Effros, R. B., . . . Tintut, Y. (2010).
553   PKA-induced receptor activator of NF-kappaB ligand (RANKL) expression in vascular

554   cells mediates osteoclastogenesis but not matrix calcification. J *Biol Chem, 285(3*9),
555   29925-29931. doi:10.1074/jbc.M110.117366
556 Wada, T., Nakashima, T., Hiroshi, N., & Penninger, J. M. (2006). RANKL-RANK signaling in
557   osteoclastogenesis   and   bone   disease.   Tr*ends   Mol   Med,   12(1*),   17-25.
558   doi:10.1016/j.molmed.2005.11.007
559 Yue, R., Zhou, B. O., Shimada, I. S., Zhao, Z., & Morrison, S. J. (2016). Leptin Receptor
560   Promotes Adipogenesis and Reduces Osteogenesis by Regulating Mesenchymal
561   Stromal Cells in Adult Bone Marrow. Ce*ll Stem Cell, 18(6*), 782-796.
562   doi:10.1016/j.stem.2016.02.015
563 Zhang, X., Xiang, L., Ran, Q., Liu, Y., Xiang, Y., Xiao, Y., . . . Li, Z. (2015). Crif1 Promotes
564   Adipogenic Differentiation of Bone Marrow Mesenchymal Stem Cells After
565   Irradiation by Modulating the PKA/CREB Signaling Pathway. St*em Cells, 33(6*),
566   1915-1926. doi:10.1002/stem.2019
567
568
569
570
571
572
573
574
575
576
577
578
579
580
581
582
583
584
585
586
587
588
589
590
591
592
593
594
595
596
597
598
599
600
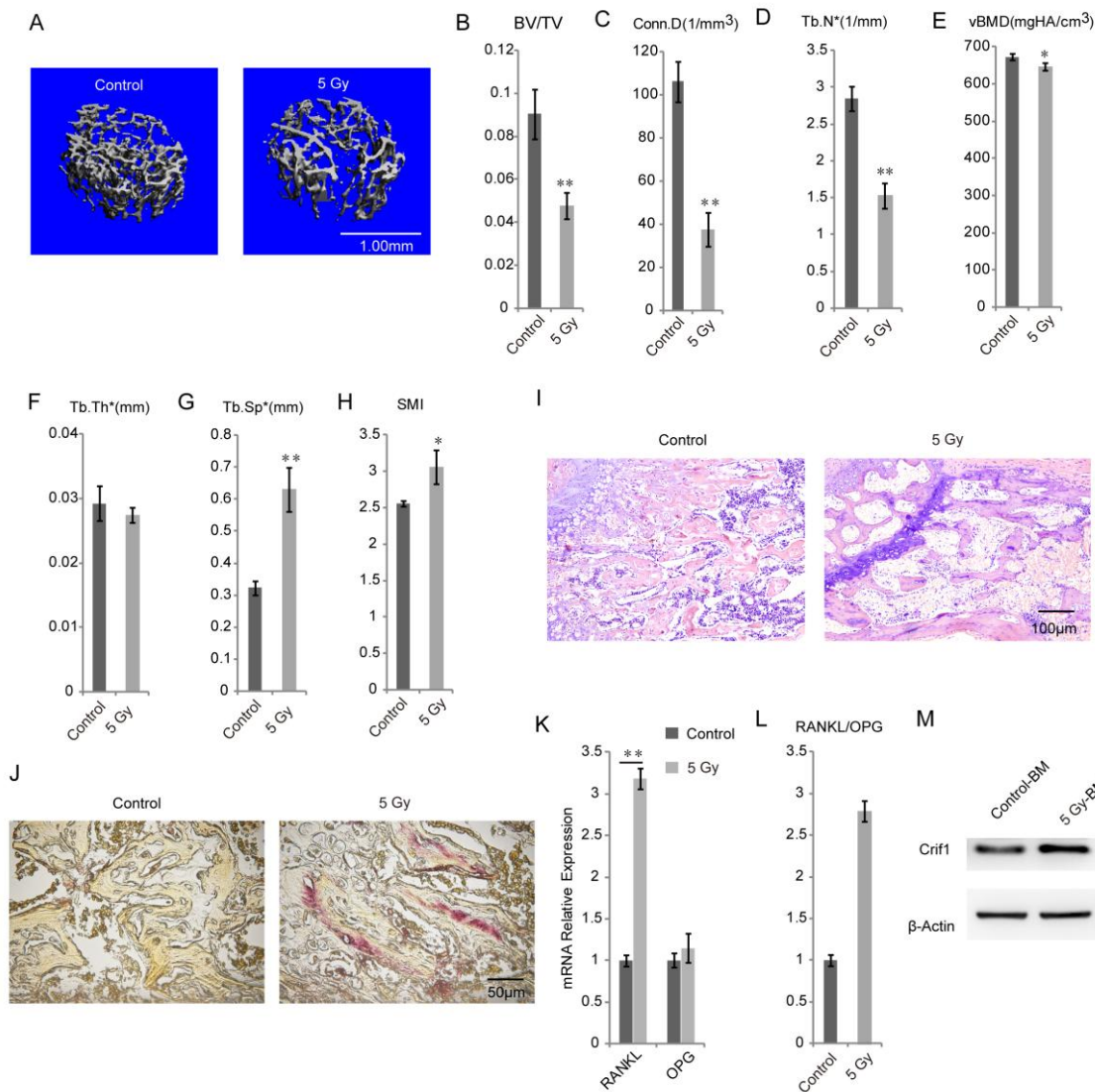
Figures:

Figure 1. Radiation induces osteoporosis in mice

(A) Micro-CT images of the distal metaphysis of the femur.

(B-H) Micro-CT analysis of the trabecular bone volume/total volume (B), connectivity density (C), trabecular number (D), bone mineral density (E), trabecular thickness (F), trabecular spacing (G), and structure model index (H).

(I) H&E staining of femoral sections from irradiated mice and controls.

(J) TRAP staining of femoral sections from irradiated mice and controls.

(K) RT-qPCR analysis of RANKL and OPG mRNA expression in flushed whole bone marrow.

(L) RANKL/OPG ratio of RT-qPCR results.

(M) Western blotting analysis of Crif1 expression in flushed whole bone marrow.

*$P < 0.05$, **$P < 0.01$. All experiments were performed in triplicate, and the bars represent the mean $\pm$ SD.

14
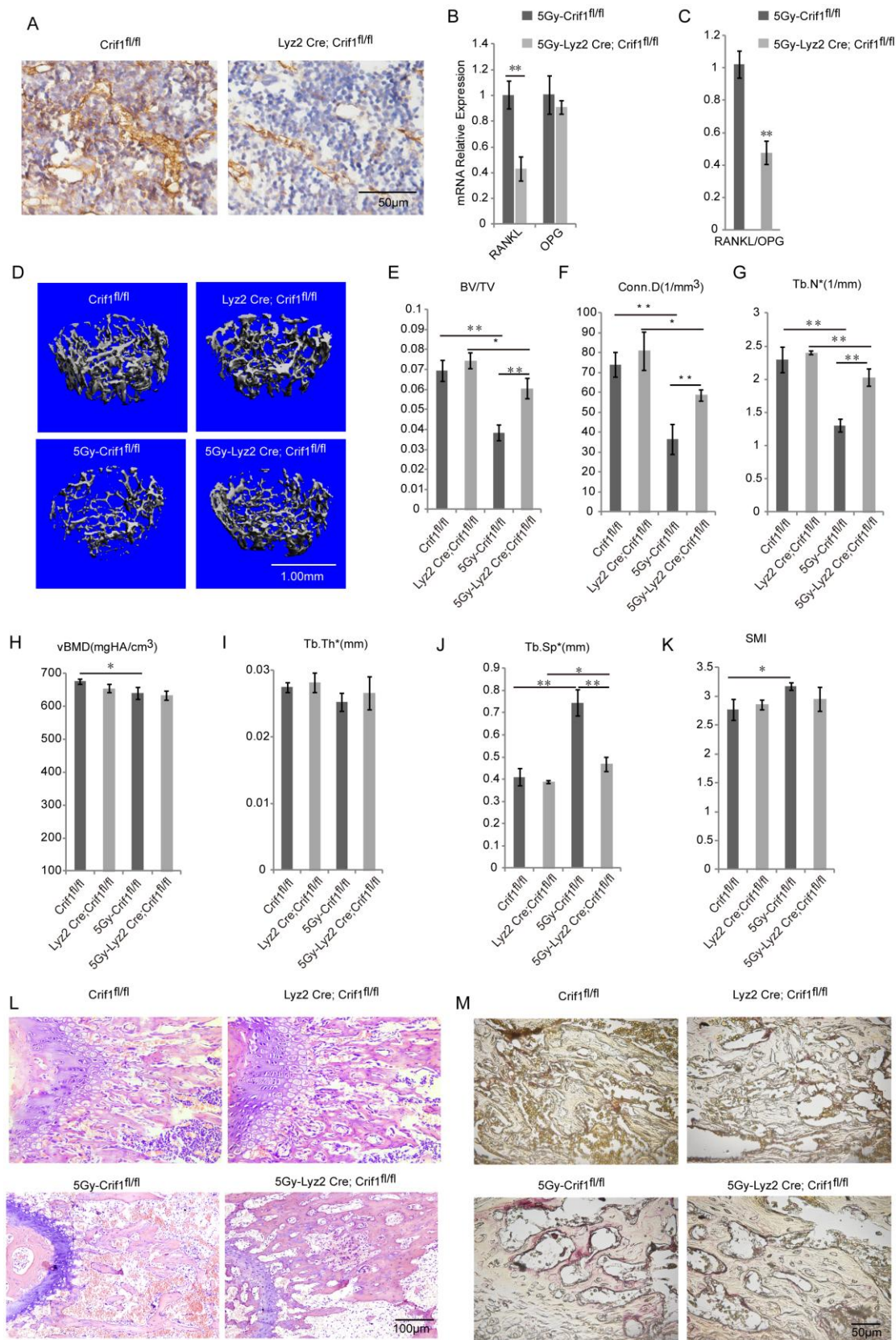
Figure 2. Conditional *Crif1* deletion from bone marrow reduces bone loss after radiation

(A) Histochemical staining analysis of Crif1 expression in femoral bone marrow.

(B) RT-qPCR analysis of RANKL and OPG mRNA expression in flushed whole bone marrow of *Crif1^{fl/fl}* mice and *Lyz2Cre;Crif1^{fl/fl}* mice after 5 Gy radiation.

625   (C) RANKL/OPG ratio of RT-qPCR results.

626   (D) Micro-CT images of the distal metaphysis of the femur from $Lyz2Cre;Crif1^{fl/fl}$ mice and

627    $Crif1^{fl/fl}$ mice.

628   (E-K) Micro-CT analysis of the trabecular bone volume/total volume (E), connectivity

629   density (F), trabecular number (G), bone mineral density (H), trabecular thickness (I),

630   trabecular spacing (J), and structure model index (K).

631   (L) H&E staining of femoral sections from $Crif1^{fl/fl}$ mice and $Lyz2Cre;Crif1^{fl/fl}$ mice.

632   (M) TRAP staining of femoral sections from $Crif1^{fl/fl}$ mice and $Lyz2Cre;Crif1^{fl/fl}$ mice.

633    $*P < 0.05$, $**P < 0.01$. All experiments were performed in triplicate, and the bars represent

634   the mean $\pm$ SD.

635

636

637

638

639

640

641

642

643

644

645

646

647

648

649

650

651

652

653

654

655

656

657
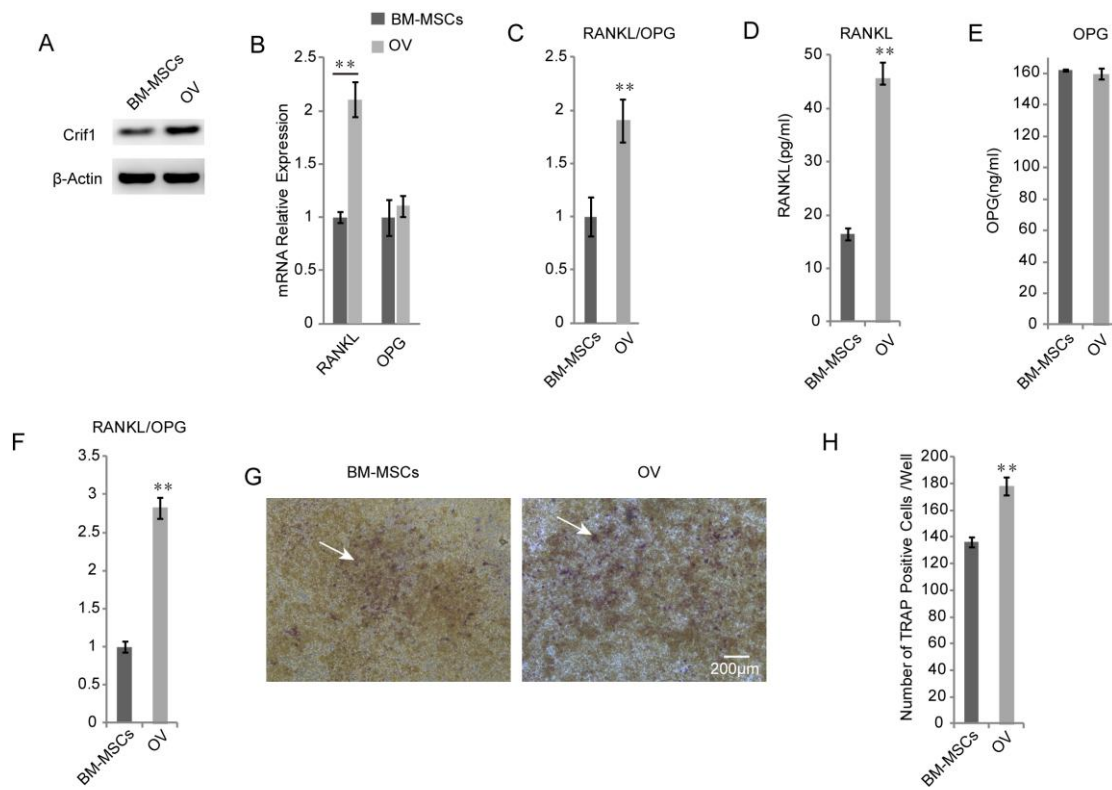
Figure 3. Overexpression of Crif1 in BM-MSCs results in increases in RANKL secretion and the ratio of RANKL to OPG

(A) Western blotting analysis of Crif1 expression in mouse BM-MSCs. Mouse BM-MSCs were transfected with a Crif1 lentiviral overexpression vector.

(B) RT-qPCR analysis of RANKL and OPG mRNA expression in BM-MSCs and Crif1-overexpressing BM-MSCs (OV). BM-MSCs and OV were cocultured with RAW264.7.

(C) RANKL/OPG ratio of RT-qPCR results.

(D) ELISA analysis of RANKL protein levels in coculture supernatant medium.

(E) ELISA analysis of OPG protein levels in coculture supernatant medium.

(F) RANKL/OPG ratio in coculture supernatant medium.

(G) TRAP staining of RAW264.7 after 7 days in coculture.

(H) Average number of TRAP-positive cells/well (arrow) from RAW264.7 cells in coculture.

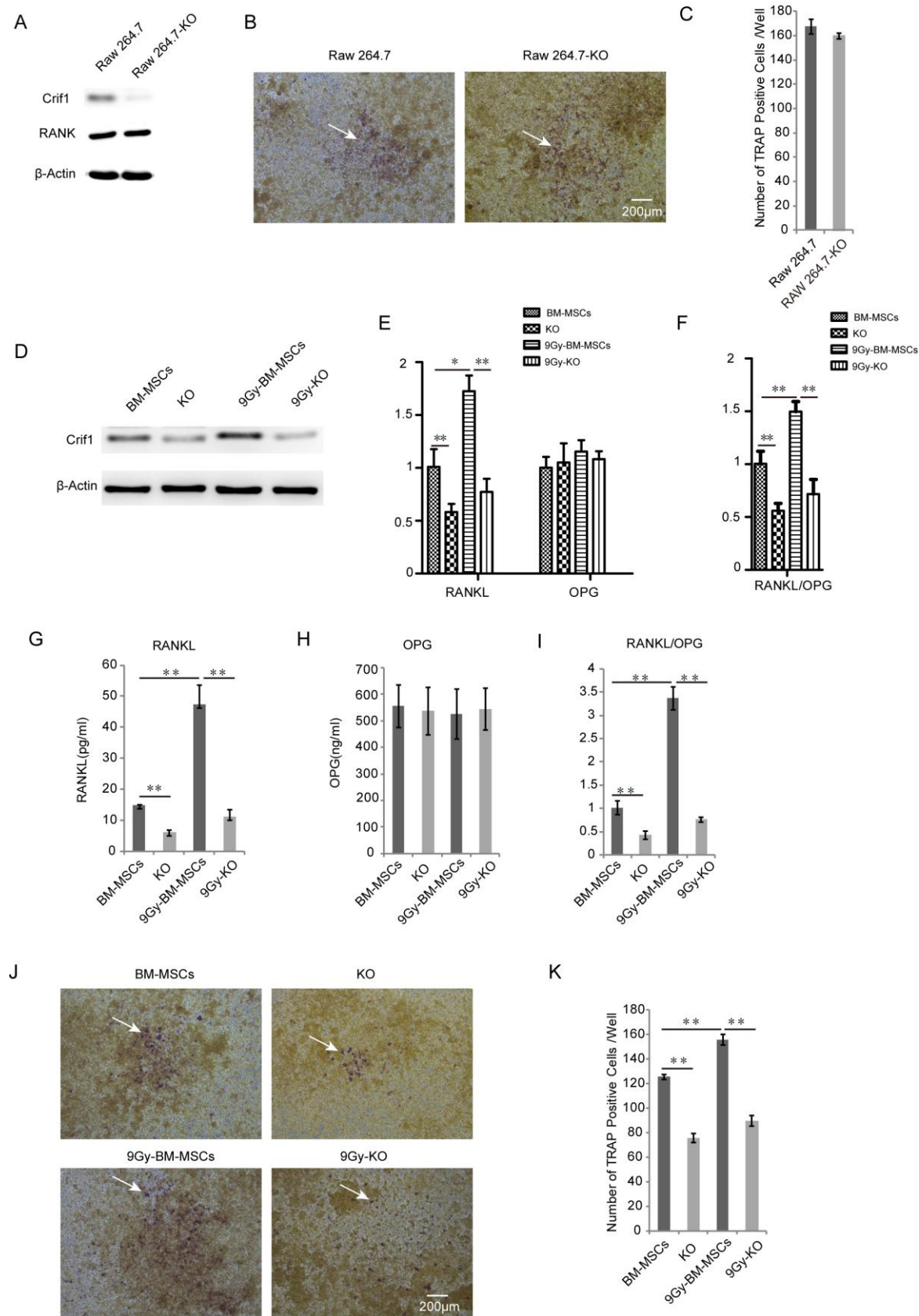*$P < 0.05$, **$P < 0.01$. All experiments were performed in triplicate, and the bars represent the mean $\pm$ SD.

17

Figure 4. Crfi1 is involved in the regulation of RANKL expression after radiation

(A) Western blotting analysis of Crif1 and RANK expression in RAW264.7 cells. Crif1 was knocked out from RAW264.7 cells (RAW264.7-KO).

(B) TRAP staining of RAW264.7-KO and controls after 7 days in coculture with mouse BM-MSCs.

18

687 (C) Average number of TRAP-positive cells/well (arrow) from RAW264.7-KO and controls
688 after 7 days in coculture with mouse BM-MSCs.
689 (D) Western blotting analysis of Crif1 expression in BM-MSCs. Crif1 was knocked out from
690 mouse BM-MSCs (KO), and KO and controls were irradiated with 9 Gy Co-60.
691 (E) RT-qPCR analysis of RANKL and OPG mRNA expression in BM-MSCs and Crif1
692 knockout BM-MSCs (KO). BM-MSCs and KO were cocultured with RAW264.7
693 (F) RANKL/OPG ratio of RT-qPCR results.
694 (G) ELISA analysis of RANKL protein levels in coculture supernatant medium.
695 (H) ELISA analysis of OPG protein levels in coculture supernatant medium.
696 (I) RANKL/OPG ratio in coculture supernatant medium.
697 (J) TRAP staining of RAW264.7 after 7 days in coculture.
698 (K) Average number of TRAP-positive cells/well (arrow) from RAW264.7 in coculture.
699 *P < 0.05*, **P < 0.01. All experiments were performed in triplicate, and the bars represent
700 the mean ± SD.
701
702
703
704
705
706
707
708
709
710
711
712
713
714
715
716
717
718
719
720
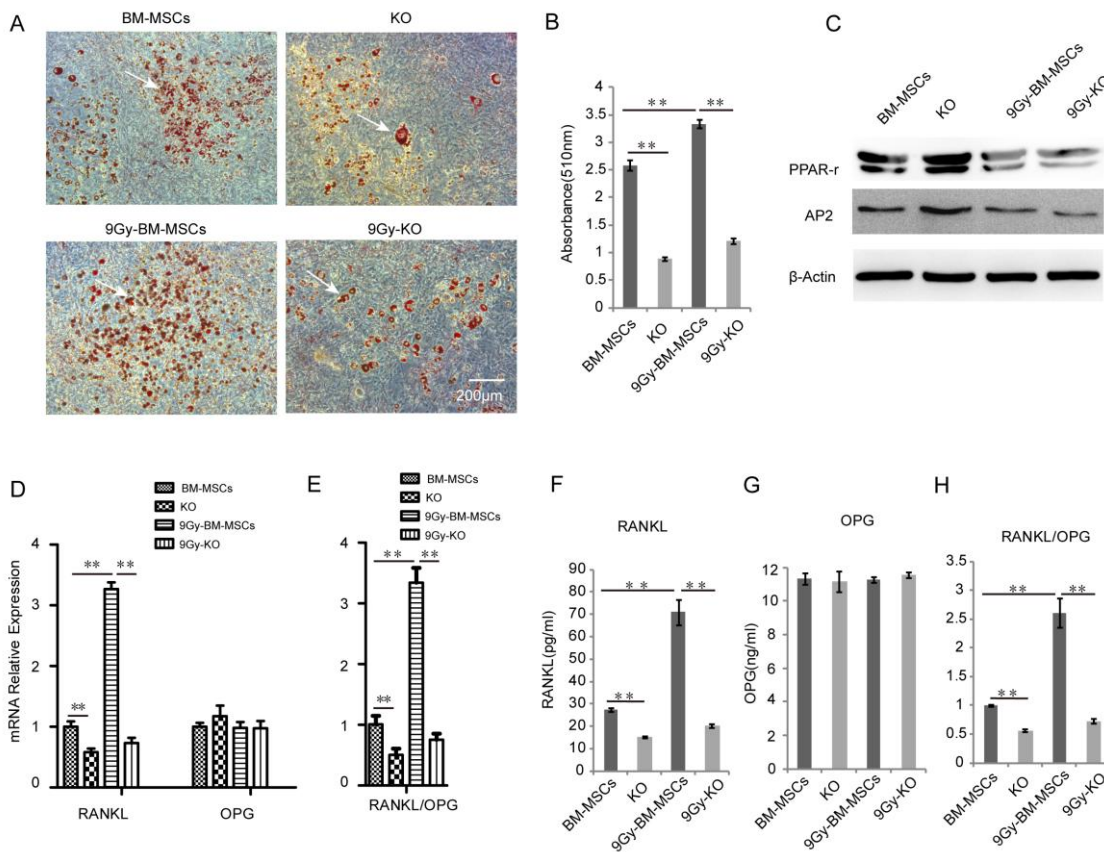
Figure 5. Crif1 mediates adipogenesis and RANKL secretion in adipocytes

(A) Oil red O staining analysis of mouse BM-MSCs after 21 days of adipogenic differentiation. Crif1 was knocked out from mouse BM-MSCs (KO), and KO and controls were irradiated with 9 Gy Co-60. KO and controls were treated with mouse mesenchymal stem cell adipogenic differentiation medium (Ad) to induce adipogenesis.

(B) The dye from oil red O staining was extracted using isopropanol, and the optical density at 510 nm was measured using a Benchmark Plus.

(C) Western blotting analysis of adipogenesis-related markers and transcription factors PPARγ and AP2 in mouse BM-MSCs after 21 days of adipogenic differentiation.

(D) RT-qPCR analysis of RANKL and OPG mRNA expression in BM-MSCs and Crif1 knockout BM-MSCs (KO).
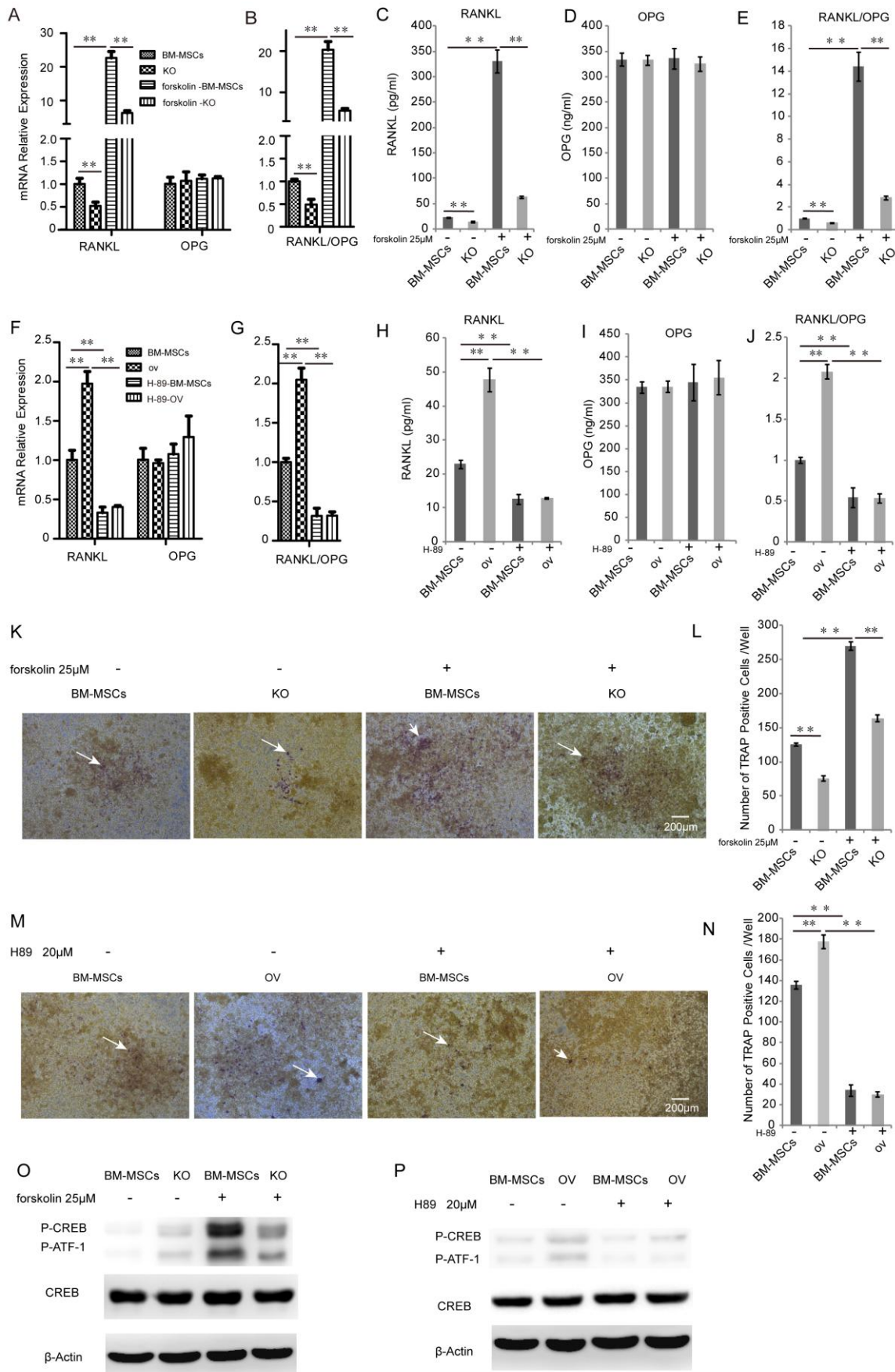
(E)RANKL/OPG ratio of RT-qPCR results.

(F) ELISA analysis of RANKL protein levels in supernatant adipogenic differentiation medium.

(G) ELISA analysis of OPG protein levels in supernatant adipogenic differentiation medium.

(H) RANKL/OPG ratio in supernatant adipogenic differentiation medium.

*$P < 0.05$, **$P < 0.01$..All experiments were performed in triplicate, and the bars represent the mean $\pm$ SD.

20

Figure 6. Crif1 promotes RANKL secretion by modulating the cAMP/PKA signalling pathway

(A) RT-qPCR analysis of RANKL and OPG mRNA expression in BM-MSCs and Crif1 knockout BM-MSCs (KO). BM-MSCs and KO were cocultured with RAW264.7 with or

21

746   without 25 μM forskolin respectively.

747   (B) RANKL/OPG ratio of RT-qPCR results.

748   (C) ELISA analysis of RANKL protein levels in coculture supernatant medium with or

749   without 25 μM forskolin.

750   (D) ELISA analysis of OPG protein levels in coculture supernatant medium with or without

751   25 μM forskolin.

752   (E) RANKL/OPG ratio in coculture supernatant medium with or without 25 μM forskolin.

753   (F) RT-qPCR analysis of RANKL and OPG mRNA expression in BM-MSCs and

754   Crif1-overexpressing BM-MSCs (OV). BM-MSCs and OV were cocultured with RAW264.7

755   with or without 20 μM H89 respectively.

756   (G) RANKL/OPG ratio of RT-qPCR results.

757   (H) ELISA analysis of RANKL protein levels in coculture supernatant medium with or

758   without 20 μM H89.

759   (I) ELISA analysis of OPG protein levels in coculture supernatant medium with or without 20

760   μM H89.

761   (J) RANKL/OPG ratio in coculture supernatant medium with or without 20 μM H89.

762   (K) TRAP staining of RAW264.7 in coculture treated with or without 25 μM forskolin.

763   (L) Average number of TRAP-positive cells/well (arrow) from RAW264.7 in coculture

764   treated with or without 25 μM forskolin.

765   (M) TRAP staining of RAW264.7 in coculture treated with or without 20 μM H89.

766   (N) Average number of TRAP-positive cells/well (arrow) from RAW264.7 in coculture

767   treated with or without 20 μM H89.

768   (O) Western blotting analysis of CREB phosphorylation levels in BM-MSCs in coculture

769   treated with or without 25 μM forskolin.

770   (P) Western blotting analysis of CREB phosphorylation levels in BM-MSCs in coculture

771   treated with or without 20 μM H89.

772   *P < 0.05*, **P < 0.01..All experiments were performed in triplicate, and the bars represent
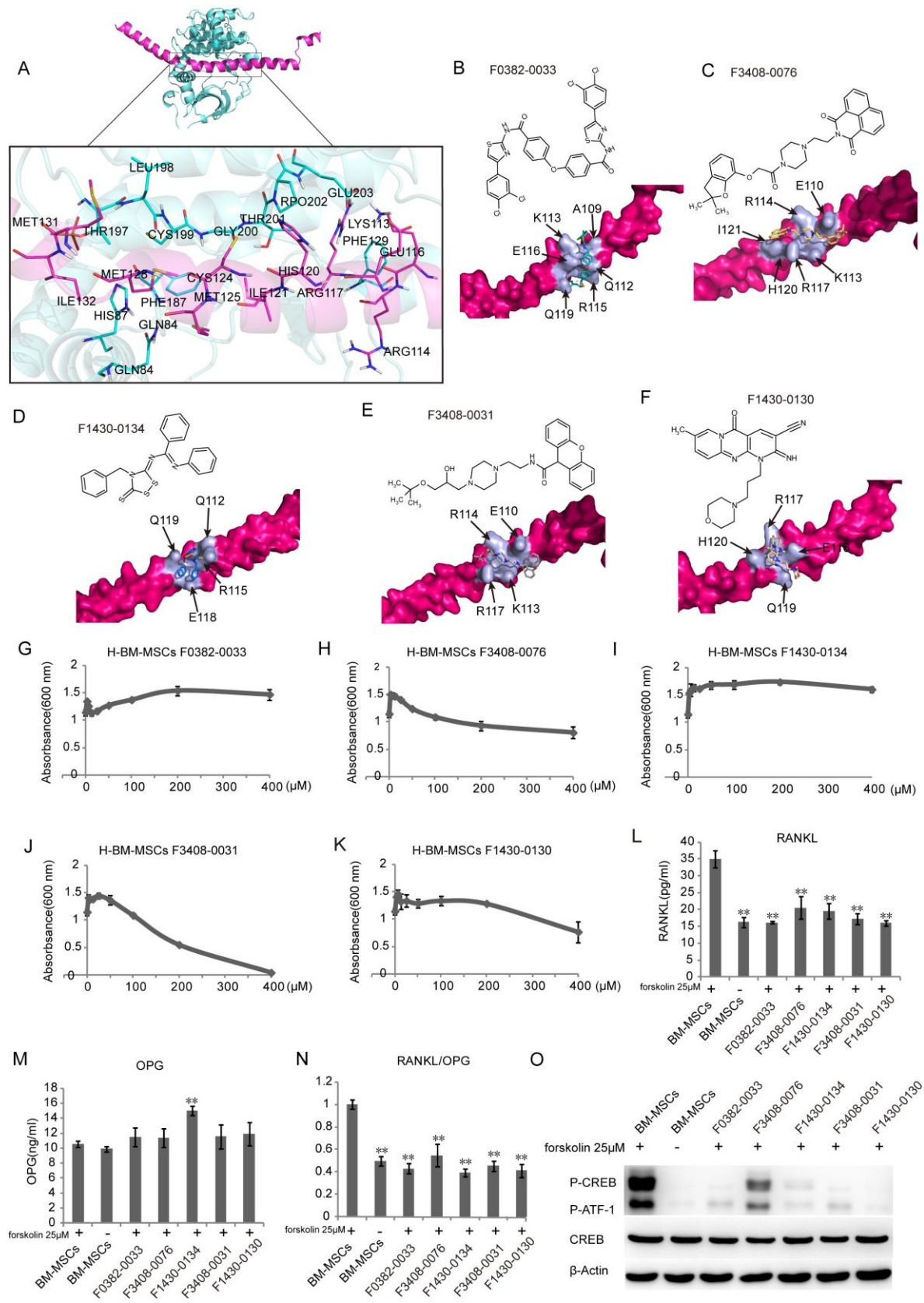
773   the mean ±SD.

Figure 7. Crif1 inhibitors effectively suppress RANKL secretion and CREB phosphorylation

(A) Crif1− PKAα interaction model showing Crif1 (colored in rose red) and PKAα (colored in cyan). Interface amino acids are shown as sticks and colored in rose red (for Crif1) and

23

781   cyan (for PKAα) and indicated as a zoomed-in view in the inset figure.

782   (B-F) Chemical structure of each inhibitor molecule and their docked pose on Crif1 (colored

783   in rose red, surface view). Docked molecule (stick) and the amino acids involved in the

784   hydrophobic interactions (light purple) are shown. F0382-0033 (B), F3408-0076 (C),

785   F1430-0134 (D), F3408-0031 (E) and F1430-0130 (F).

786   (G-K) A tetrazolium salt (WST-8) assay was carried out to study the toxity effect of

787   compounds on the hBM-MSCs. F0382-0033 (G), F3408-0076 (H), F1430-0134 (I),

788   F3408-0031 (J) and F1430-0130 (K).

789   (L) ELISA analysis of RANKL protein levels in supernatant medium. hBM-MSCs were

790   pretreated with 5 different compounds followed by treatment with forskolin, and supernatant

791   medium was collected for ELISA after 3 days.

792   (M) ELISA analysis of OPG protein levels in supernatant medium.

793   (N) RANKL/OPG ratio in supernatant medium.

794   (O) Western blotting analysis of CREB phosphorylation levels. hBM-MSCs were pretreated

795   with 5 different compounds followed by treatment with forskolin and total protein lysates

796   were extracted for CREB phosphorylation detection after 1 hour.

797   *P < 0.05, **P < 0.01*. All experiments were performed in triplicate, and the bars represent

798   the mean ±SD.

799

800

801

802

803

804

805

806

807

808

809

810

811

812

813

814

815

816

817

818

819

820

821

822

823

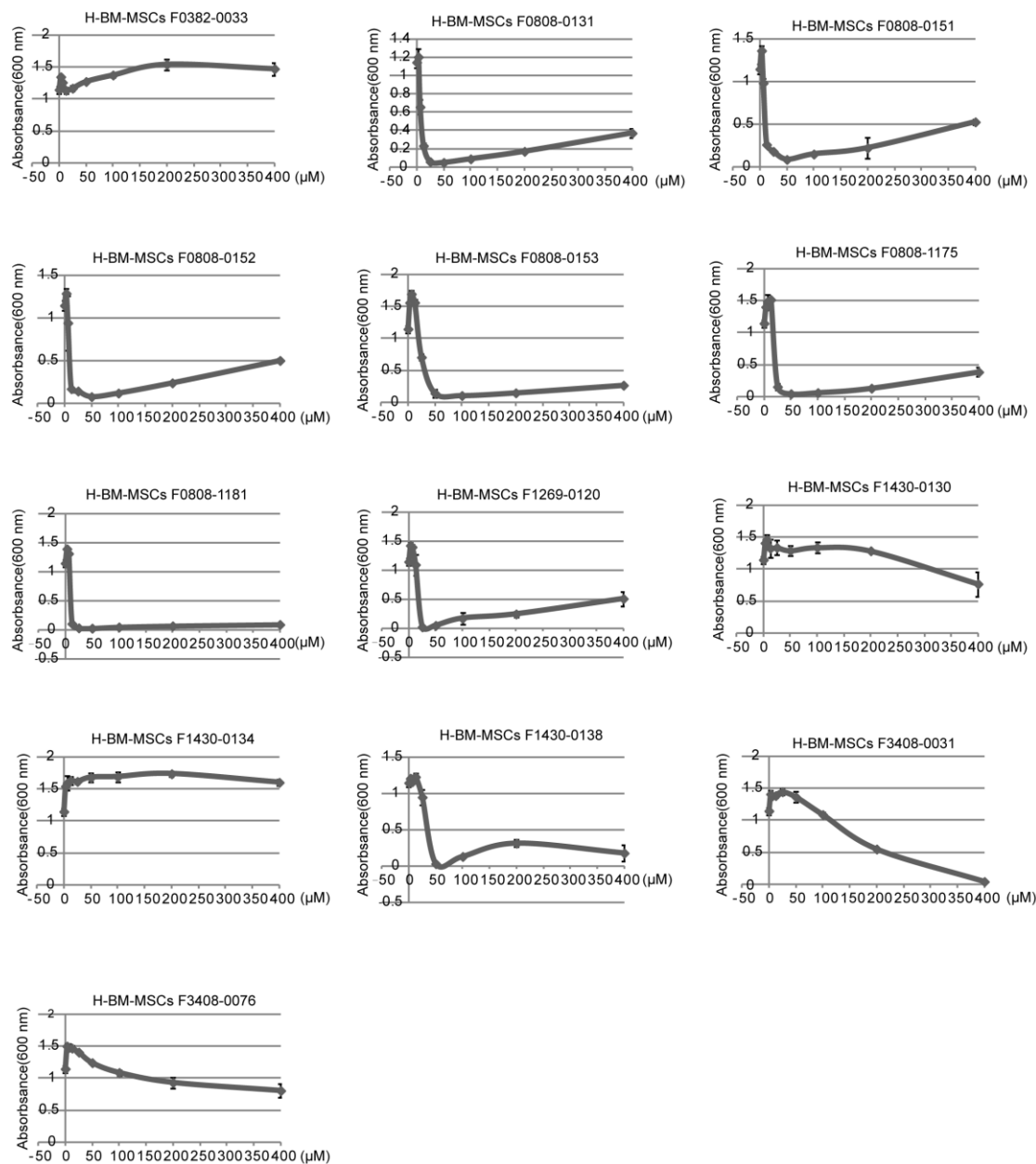824

825

826

827

828 **Supplementary data**

829

830

Compound Name	Affinity (kcal/mol)
F3408-0076	-14.6
F0382-0033	-13.1
F1430-0130	-12.9
F0808-0153	-12.5
F0808-0131	-12.5
F0808-0151	-12.4
F0808-1181	-12.4
F0808-1175	-12.4
F1269-0120	-12.3
F0808-0152	-12.2
F3408-0031	-12.2
F1430-0134	-12
F1430-0138	-12

831

832

833   Table S1. 13 compounds were chosen based on binding energy <-12.0 kcal/mol.
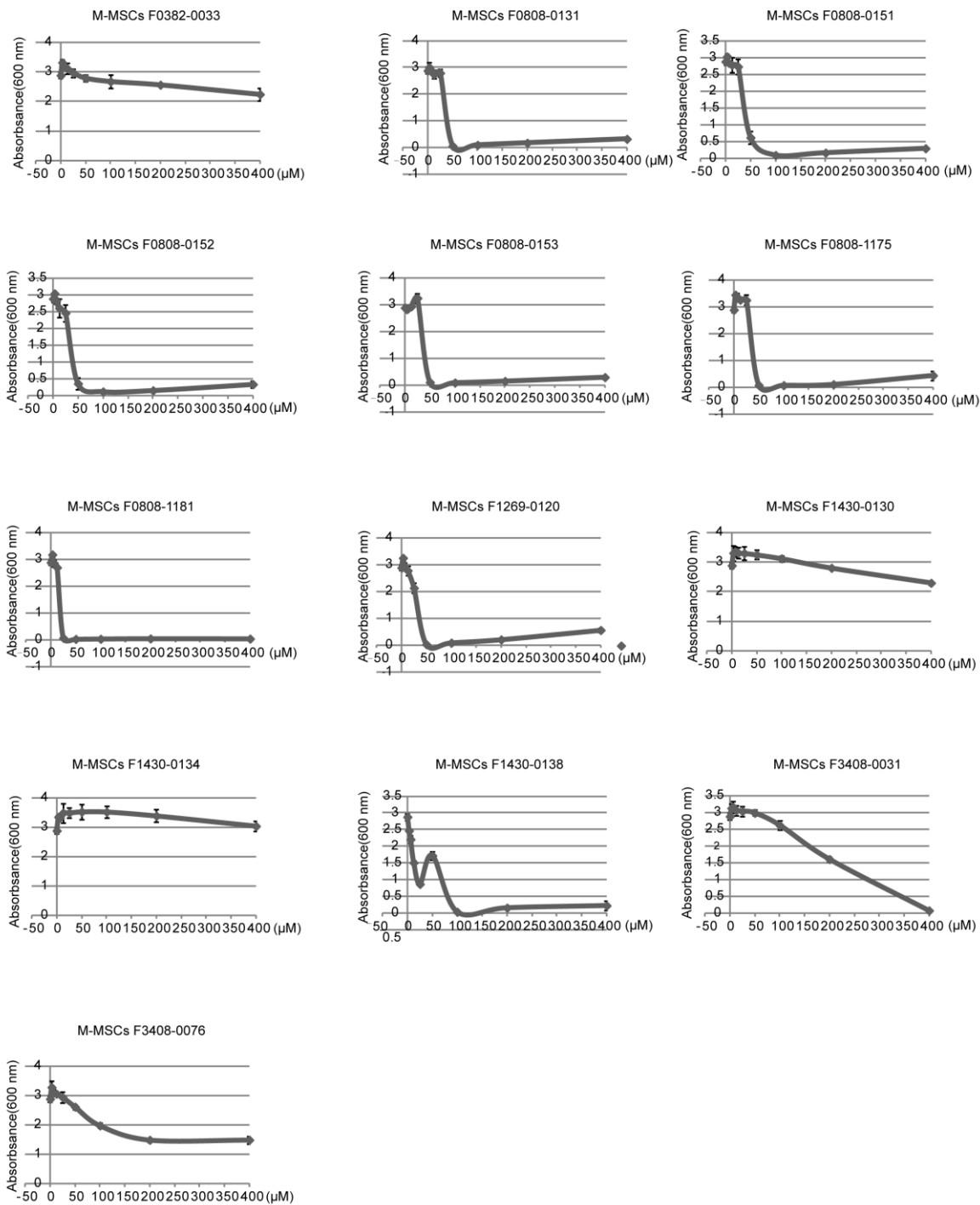
834

835
836
837 Figure S1. A tetrazolium salt (WST-8) assay was carried out to study the toxic effects of
838 compounds on H –BM-MSCs.
839
840
841
842
843
844
845
846
847

26

848
849
850 Figure S2. A tetrazolium salt (WST-8) assay was carried out to study the toxic effects of
851 compounds on vero cells.
852
853
854
855

Figure S3. A tetrazolium salt (WST-8) assay was carried out to study the toxic effects of compounds on mouse BM-MSCs.